Electronic Supplementary Information

A fluorescent probe based on novel fused four ring quinoxalinamine for palladium detection and bio-imaging

Yong Zhang, Min Yang and Min Ji*

School of Biological Science and Medical Engineering, Southeast University, Nanjing, 210009, P. R. China

Corresponding Author E-mail: jimin@seu.edu.cn

Table of content

1. Fluorescence quantum yields measurement

The quantum yields were determined by using coumarin-153 in ethanol (Φ = 0.38) as a standard.[1] The emission spectra of dilute sample solutions with an O.D. < 0.05 at the λ_{ex} were recorded. The quantum yield values were calculated according to the following equation:

$$\Phi_s = \frac{I_s}{I_{ref}} \cdot \frac{O.D._{ref}}{O.D._s} \cdot \left(\frac{n_s}{n_{ref}}\right)^2 \cdot \Phi_{ref}$$

Where, Φ is the quantum yield; I is the integrated emission intensity (peak area); O.D. is the absorbance at λ_{ex}; n is the refractive index. Sample and reference are denoted by s and ref, respectively.

2. Determination of the detection limit

The detection limit was calculated from fluorescence titration. In the absence of palladium, the fluorescence emission spectra of probe **QX9A-Pd** were measured by ten times and the standard deviation of the blank measurement was achieved. To gain the slop, the fluorescence intensity at 532 nm was plotted to the concentrations of palladium. The detection limit was calculated according to equation showing below:

$$\text{Detection limit} = \frac{3\sigma}{\text{k}}$$

Where σ is the standard deviation of the blank measurement, k is the slope between the fluorescence intensities versus the concentrations of palladium.

3. The synthetic details and data for characterizations of the intermediates

3.1 Synthesis of compound **1**

The 3*H*-indole **1** used in the experiment was prepared according to the reported literatures.[2-4] 4-(Trifluoromethyl)phenylhydrazine hydrochloride (12.76 g, 60 mmol) and 3-methyl-2-butanone (7.75g, 90 mmol) were dissolved in acetic acid (90 mL). Then the resulting mixture was heated to 90 ºC and stirred for 12 hours. After the reaction was completed (monitored by TLC), the hot solution was cooled to room temperature. With water added to the solution, the mixture was extracted with ethyl acetate (3 times). The combined organic layers were washed with saturated $NaHCO_3$ solution and brine solution, then dried by Na_2SO_4 and evaporated in vacuum to afford the crude product, which was used for the next step without further purification.

3.2 Synthesis of compound **2**

The indolium iodide **2** was prepared according to the reported literatures. [3, 4] To the crude 3*H*-indole **1** in THF (120 mL), iodomethane (17g, 120 mmol) was added. The solution was refluxed at 70 ºC for 12 h and a large amount of insoluble solid precipitated from the solution. Then, the mixture was cooled to 0 ºC in an ice-bath and filtered. The solid was washed with cold THF after filtration. After dried under vacuum, light yellow solid (12.2 g, 55%) was obtained.

3.3 Synthesis of intermediates **QX8N** and **QX9N**

The compounds were prepared according to our previous work.[5] A mixture of compound **2** (5.55 g, 15 mmol), 4-nitro-*o*-phenylenediamine (2.76g, 18 mmol) and iodine (11.42 g, 45 mmol) in DMSO (45 mL) was stirred at 100 ºC for 1 h. After the reaction was completed (monitored by TLC), the mixture was cooled to room temperature and quenched with saturated $Na_2S_2O_3$ aqueous, then extracted with ethyl acetate. The combined organic layers were washed with brine solution, dried over anhydrous Na_2SO_4 and evaporated in vacuum. The residue was purified by column chromatography on silica gel with petroleum ether: ethyl acetate (400:1, v/v) as eluent to afford a pair of isomers.

QX8N: yellow solid (1.75 g, 30%). mp 214-215 ºC; ^{1}H NMR (400 MHz, $CDCl_3$) δ 8.75 (d, *J* = 2.4 Hz, 1H), 8.28 (dd, *J* = 9.0, 2.4 Hz, 1H), 8.10 (d, *J* = 9.0 Hz, 1H), 7.77 (s, 1H), 7.64 (d, *J* = 8.5 Hz, 1H), 7.25 (d, *J* = 8.6 Hz, 1H), 3.83 (s, 3H), 1.81 (s, 6H); ^{13}C NMR (100 MHz, $CDCl_3$) δ 153.6, 147.9, 146.4, 141.8, 141.1, 139.9, 131.8, 129.8, 125.1 (d, $J_{C\text{-}F}$ = 3.8 Hz), 124.9 (q, $J_{C\text{-}F}$ = 33 Hz), 124.3 (q, $J_{C\text{-}F}$ = 270 Hz), 123.0, 122.7 (d, $J_{C\text{-}F}$ = 3.6 Hz), 119.3, 113.9, 41.2, 31.3, 28.5; HRMS (ESI$^+$) calcd for $C_{19}H_{15}F_3N_4O_2$ [M+H]$^+$ 389.12199, found 389.12212.
QX9N: yellow solid (2.04 g, 35%). mp 190-191 ºC; ^{1}H NMR (400 MHz, $CDCl_3$) δ 8.90 (d, *J* = 2.3 Hz, 1H), 8.43 (dd, *J* = 9.1, 2.4 Hz, 1H), 7.92 (d, *J* = 9.1 Hz, 1H), 7.78 (s, 1H), 7.64 (d, *J* = 8.4 Hz, 1H), 7.27 (d, *J* = 8.6 Hz, 1H), 3.85 (s, 3H), 1.81 (s, 6H); ^{13}C NMR (100 MHz, $CDCl_3$) δ 152.6, 146.7, 144.8, 144.4, 140.8, 137.5, 132.2, 127.8, 125.2 (q, $J_{C\text{-}F}$ = 33 Hz), 125.1 (d, $J_{C\text{-}F}$ = 4.0 Hz), 125.0, 124.3 (q, $J_{C\text{-}F}$ = 270 Hz), 123.4, 122.9 (d, $J_{C\text{-}F}$ = 4.0 Hz), 114.1, 41.1, 31.4, 28.7; HRMS (ESI$^+$) calcd for $C_{19}H_{15}F_3N_4O_2$ [M+H]$^+$ 389.12199, found 389.12210.

3.4 Synthesis of intermediates **QX8A** and **QX9A**

A mixture of **QX8N** or **QX9N** (1.94 g, 5.0 mmol), reduced iron powder (3.35 g, 60 mmol), NH_4Cl (3.75 g, 70 mmol), H_2O (30 mL) and EtOH (30 mL) was stirred at 90 ºC for 12 hours. After the reaction was completed (monitored by TLC), the reaction mixture was cooled to room temperature and the solvent was removed. Then the residue was extracted with ethyl acetate. The combined organic layers were washed with brine, dried over anhydrous Na_2SO_4 and evaporated in vacuum. The residue was purified by column chromatography on silica gel with petroleum ether: ethyl acetate (20:1, v/v) as eluent to afford the corresponding product **QX8A** or **QX9A**.

QX8A: yellow solid (1.58 g, 88%). mp 201-202 ºC; ^{1}H NMR (400 MHz, $CDCl_3$) δ 7.75 (d, *J* = 8.7 Hz, 1H), 7.70 (s, 1H), 7.53 (d, *J* = 8.5 Hz, 1H), 7.11 (d, *J* = 8.6 Hz, 1H), 6.97 (d, *J* = 2.3 Hz, 1H), 6.91 (dd, *J* = 8.8, 2.4 Hz, 1H), 4.02 (s, 2H), 3.71 (s, 3H), 1.71 (s, 6H); ^{13}C NMR (100 MHz, $CDCl_3$) δ 147.7, 145.5, 145.4, 142.1, 133.8, 132.5, 129.6, 124.6 (q, $J_{C\text{-}F}$ = 270 Hz), 124.5 (d, *J* = 3.7 Hz), 123.7 (q, $J_{C\text{-}F}$ = 32 Hz), 122.5 (d, *J* = 3.6 Hz), 117.2, 113.2, 107.4, 40.2, 31.0, 28.6; HRMS (ESI$^+$) calcd for $C_{19}H_{17}F_3N_4$ [M+H]$^+$ 359.14781, found 359.14772.
QX9A: yellow solid (1.61 g, 90%). mp 215-216 ºC; ^{1}H NMR (400 MHz, $CDCl_3$) δ 7.69 (s, 1H), 7.67 (d, *J* = 8.8 Hz, 1H), 7.53 (d, *J* = 8.5 Hz, 1H), 7.16 (d, *J* = 2.5 Hz, 1H), 7.12-7.04 (m, 2H), 3.91 (s, 2H), 3.70 (s, 3H), 1.72 (s, 6H); ^{13}C NMR (100 MHz, $CDCl_3$) δ 149.6, 144.8, 143.4, 142.4, 140.5, 134.6, 131.9, 127.7, 124.7 (q, $J_{C\text{-}F}$ = 270 Hz), 124.6 (d, *J* = 3.8 Hz), 123.3 (q, $J_{C\text{-}F}$ = 32 Hz), 122.5 (d, *J* = 3.7 Hz), 120.9, 112.9, 109.8, 40.6, 31.0, 28.3; HRMS (ESI$^+$) calcd for $C_{19}H_{17}F_3N_4$ [M+H]$^+$ 359.14781, found 359.14861.

4. Comparisons between probe QX8A-Pd and QX9A-Pd

According to the detection mechanism, the probes finally converted into the corresponding fluorophores (Scheme 2). So the greater the difference between the probes and the fluorophores in fluorescence intensity, the higher signal-to-noise ratio and more favorable to the detection of palladium.

4.1 Comparisons between the two fluorophores

Preliminary studies demonstrated that the fluorophores and corresponding probes (**QX8A**/**QX8A-Pd** and **QX9A**/**QX9A-Pd**) have distinct changes in both absorption and emission spectra (Fig. S1 and S2, ESI). The fluorescence intensity of fluorophore **QX9A** was 144 times higher than its corresponding probe **QX9A-Pd**, while **QX8A** was only 6 times higher than **QX8A-Pd** (Fig. S1 and S2, ESI). Moreover, the emission spectra of **QX8A** and **QX8A-Pd** were overlapped seriously, greatly interfering the detection performance. The fluorescence quantum yield of **QX9A** was higher than **QX8A** (Table S1, ESI). It is tentatively suggested that probe **QX9A-Pd** was better than **QX8A-Pd**.

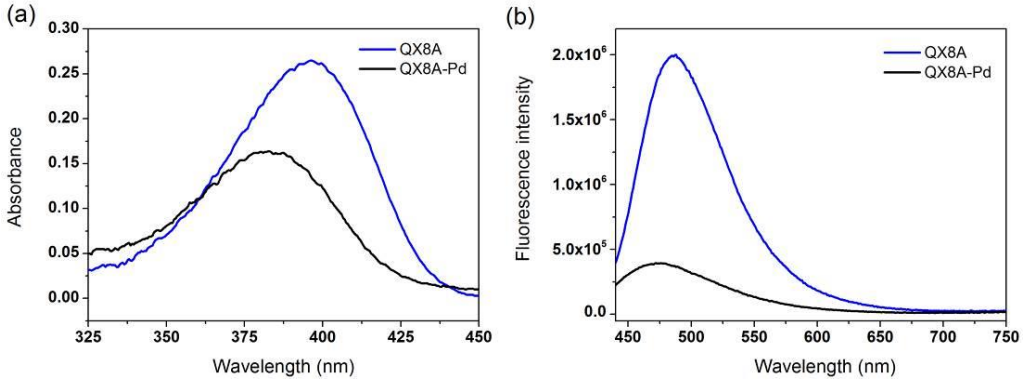

Fig. S1 The absorption and fluorescence spectra of **QX8A-Pd** and **QX8A** (10 μM) in PEG400/PBS buffer (60: 40, v/v, 10 mM, pH 7.4).

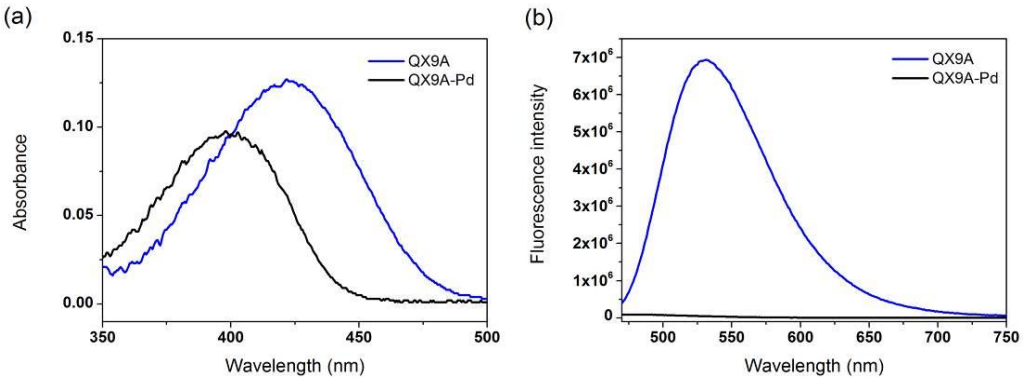

Fig. S2 The absorption and fluorescence spectra of **QX9A-Pd** and **QX9A** (10 μM) in PEG400/PBS buffer (60: 40, v/v, 10 mM, pH 7.4).

Table S1 Summary of photophysical properties of fluorophores

Compound	λ_{abs} (nm)	λ_{em} (nm)	Stokes shift (nm)	$\Phi^{[a]}$
QX8A	397	486	89	0.15
QX9A	421	531	110	0.43

[a] Quantum yields were determined by using coumarin-153 (Φ= 0.38) in ethanol as the reference standard.[1] The experiments were performed in PEG400/PBS solutions (60: 40, v/v, 10 mM PBS buffer, pH 7.4).

4.2 The responses of probes towards Pd(0)

Then, the optical responses of probe **QX8A-Pd** and **QX9A-Pd** (10 μM) towards Pd(0) were examined in PBS buffer and PEG400 solutions (PBS: PEG400 = 40: 60, v/v) at 37 ºC. As shown in Fig. 1 and Fig. S3, the absorbance of the resulting solutions both increased after addition of Pd(0). However, the fluorescence intensity of **QX9A-Pd** increased 77-folds in the presence of Pd(0), while **QX8A-Pd** increased only 4-folds. The color change of **QX8A-Pd** solutions were nearly indistinguishable, whether under visible light or 365 nm UV lamp (the inset of Fig. S3a and S3b, ESI). **QX9A-Pd** solution changed from colorless to yellow, allowing a convenient colorimetric detection by the naked eye (the inset of Fig. 1a). Meanwhile, a marked fluorescent color change of **QX9A-Pd** solution can be easily visualized under a 365 nm light (the inset of Fig. 1b). As a consequence, only probe **QX9A-Pd** was characterized in the subsequent experiments.

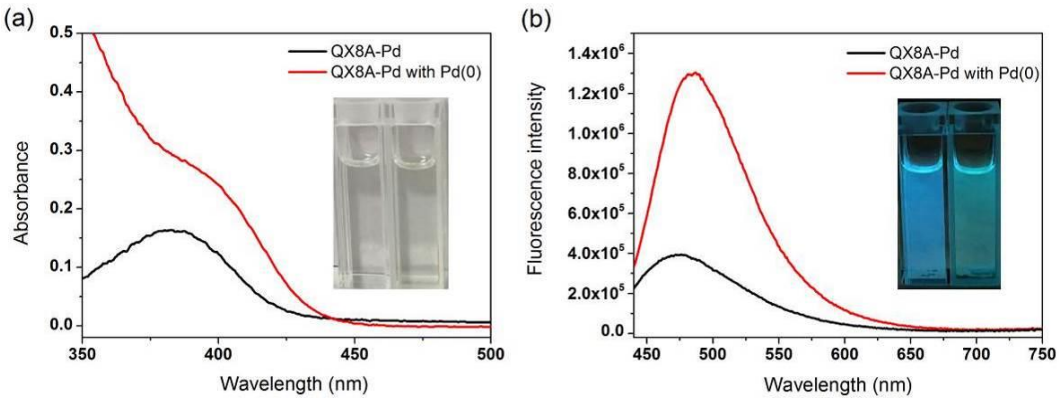

Fig. S3 Absorption (a) and fluorescence spectra (b) changes of probe **QX8A-Pd** (10 μM) upon addition of Pd(0) (100 μM) in pH= 7.4 PBS buffer and PEG400 solutions (PBS: PEG400 = 40: 60, v/v) at 37 ºC for 1 h. Inset image: colour changes under visible-light (Left) and under 365 nm UV lamp (Right). λ_{ex}= 430 nm, slit: 2 nm/2 nm.

5. The sensing behavior of QX9A-Pd for $PdCl_2$ and K_2PdCl_6

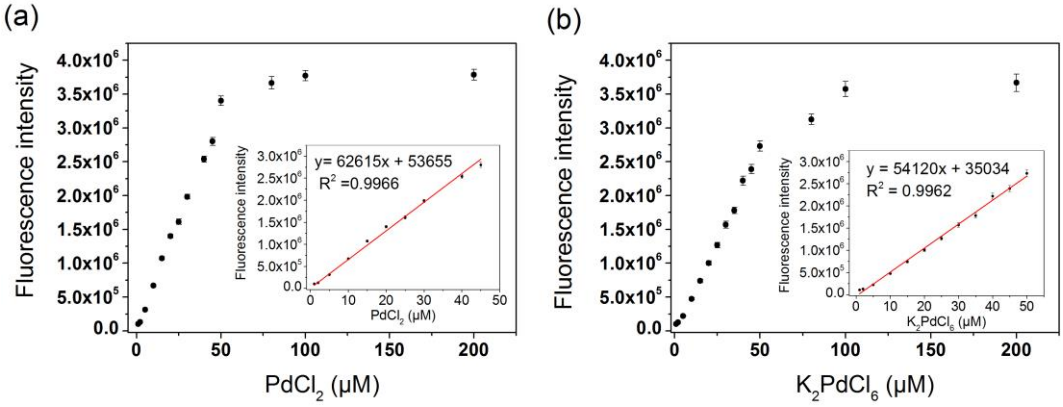

Fig. S4 The fluorescence intensity changes of probe **QX9A-Pd** (10 μM) at 532 nm in the presence of different concentrations of (a) $PdCl_2$ and (b) K_2PdCl_6 (0-200 μM) in pH= 7.4 PBS buffer and PEG400 solutions (PBS: PEG400 = 40: 60, v/v) at 37 °C for 1 h. Inset: the correlation curve of fluorescence intensity changes at 532 nm with $PdCl_2$ and K_2PdCl_6. λ_{ex}= 460 nm, slits: 2 nm/2 nm.

6. Color changes after detecting various metal ions

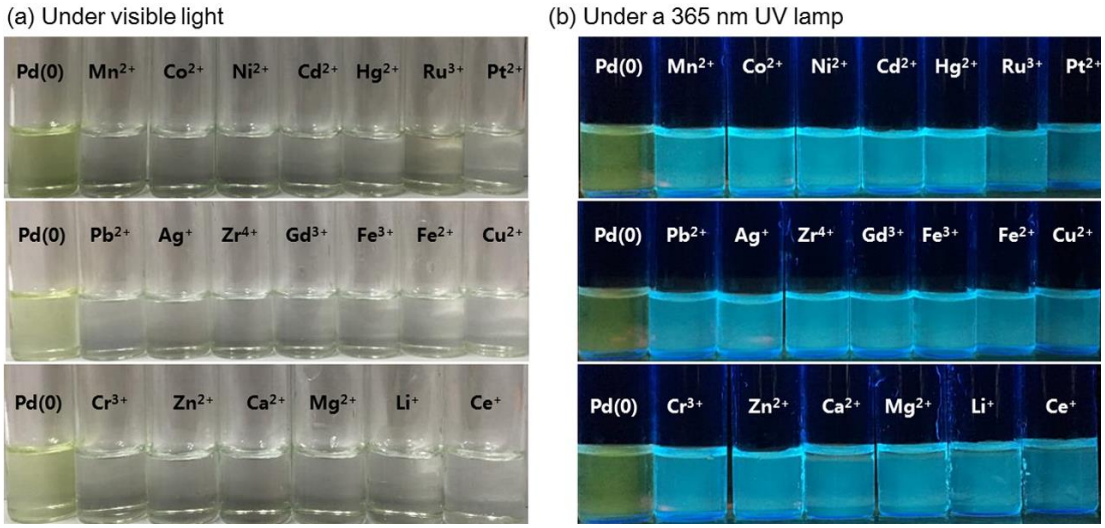

Fig. S5 (a) Colour changes of probe **QX9A-Pd** (10 uM) under visible-light and (b) under 365 nm UV lamp upon addition of different analytes (100 μM) in pH= 7.4 PBS buffer and PEG400 solutions (PBS: PEG400 = 40: 60, v/v) at 37 ºC for 1 h.

7. Competition experiments

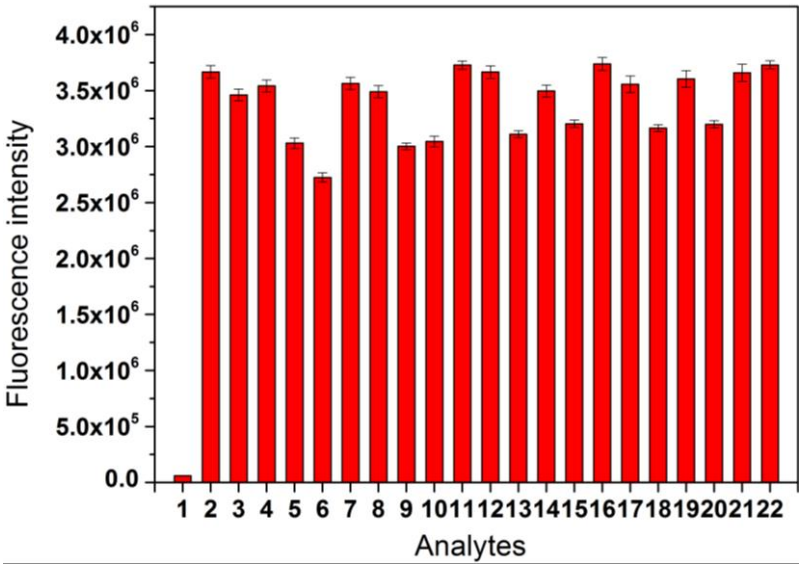

Fig. S6 Fluorescence responses of probe **QX9A-Pd** (10 uM) to Pd(0) (100 μM) in the presence of other metal ions (100 μM) in pH= 7.4 PBS buffer and PEG400 solutions (PBS: PEG400 = 40: 60, v/v) at 37 °C for 1 h (1-22: blank, Pd(0), Pt^{2+}, Ru^{3+}, Hg^{2+}, Cr^{3+}, Cd^{2+}, Ni^{2+}, Co^{3+}, Mn^{2+}, Pb^{2+}, Ag^{+}, Zr^{4+}, Gd^{3+}, Fe^{3+}, Fe^{2+}, Cu^{2+}, Zn^{2+}, Ca^{2+}, Mg^{2+}, Li^{+} and Cs^{+}, respectively). λ_{ex}= 460 nm, slits: 2 nm/2 nm.

8. The effect of PEG400 on detection

The palladium complexes containing organic ligands had poor solubilities in aqueous media, which resulted in the use of high content of DMSO (50%) in the experiments.

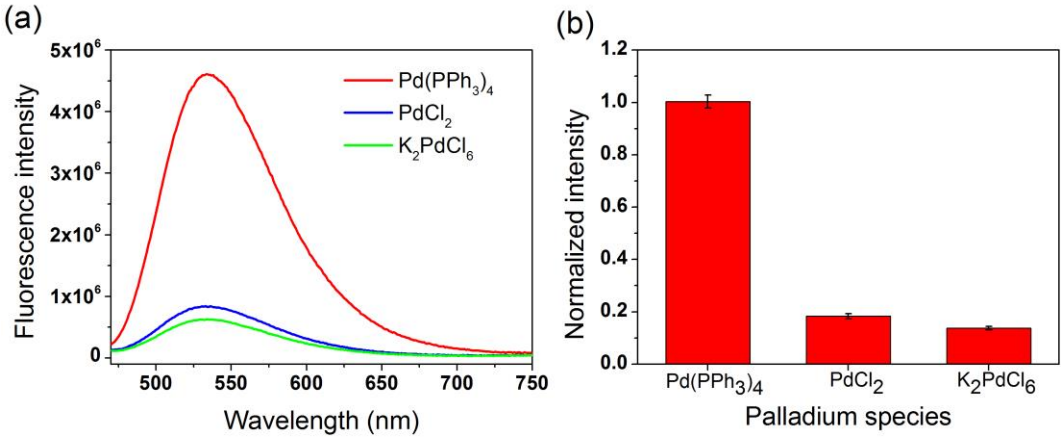

Fig. S7 (a) Fluorescence spectra changes and (b) fluorescence intensity changes of probe **QX9A-Pd** at 532 nm when detecting palladium species in the absence of PEG400. Each spectrum was obtained in DMSO/PBS buffer solution (1: 1, v/v, pH= 7.4, 10 mM) at 37 °C for 1 h. λ_{ex}= 460 nm, slits: 2 nm/2 nm.

9. The sensing behavior of QX9A-Pd for different palladium sources in the presence or absence of $NaBH_4$

9.1 Detection of $Pd(PPh_3)_4$

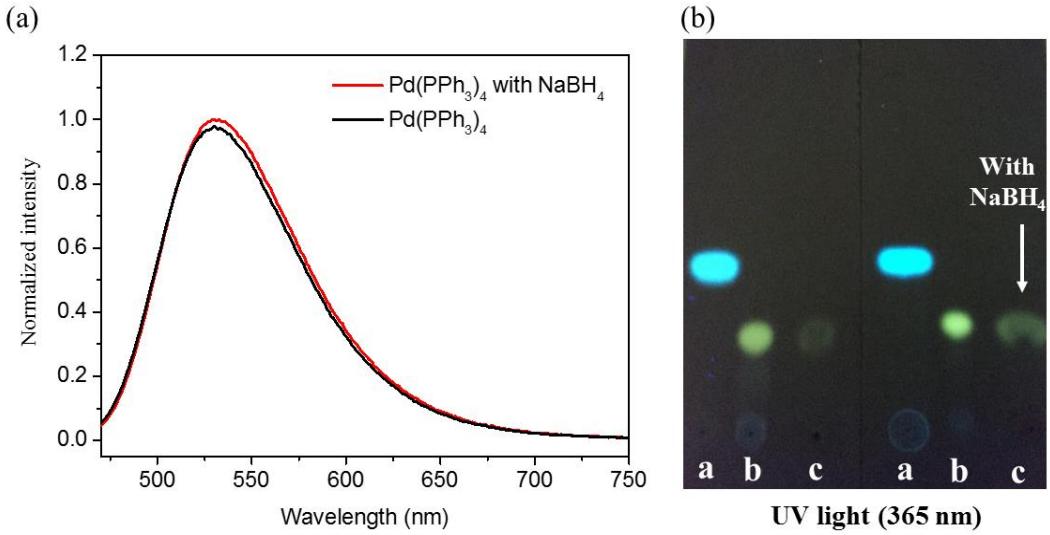

Fig. S8 (a) Fluorescence spectra changes of probe **QX9A-Pd** in the presence or absence of $NaBH_4$ when detecting $Pd(PPh_3)_4$. Each spectrum was obtained in pH= 7.4 PBS buffer and PEG400 solutions (PBS: PEG400 = 40: 60, v/v) at 37 ºC for 1 h. λ_{ex}= 460 nm, slits: 2 nm/2 nm. (b) Pictures of TLC plates under 365 nm light. Spots (a~c) on the TLC plates were probe **QX9A-Pd**, fluorophore **QX9A** and reaction mixture of probe with $Pd(PPh_3)_4$, respectively.

9.2 Detection of $Pd(PPh_3)_2Cl_2$

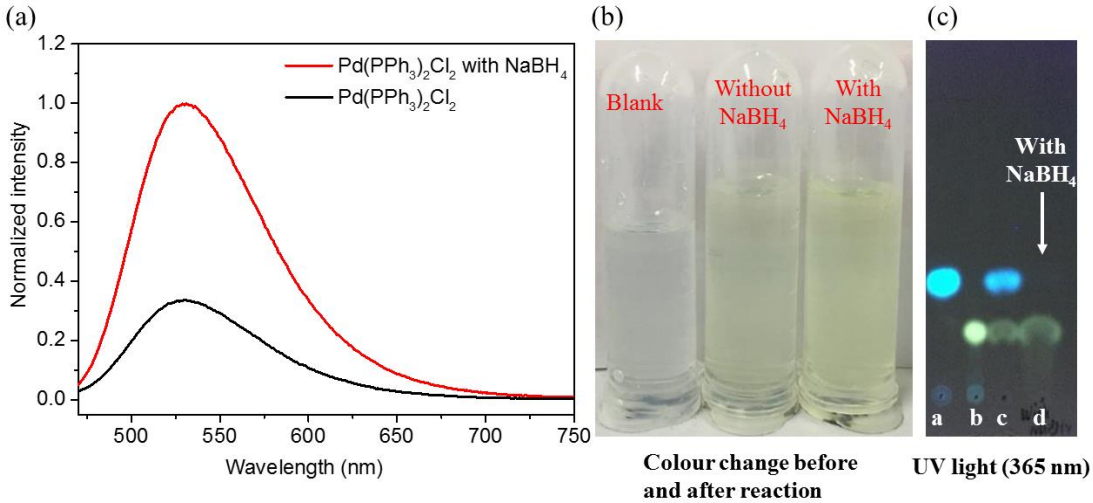

Fig. S9 (a) Fluorescence spectra changes of probe **QX9A-Pd** in the presence or absence of $NaBH_4$ when detecting $Pd(PPh_3)_2Cl_2$. Each spectrum was obtained in pH= 7.4 PBS buffer and PEG400 solutions (PBS: PEG400 = 40:60, v/v) at 37 ºC for 1 h. λ_{ex}= 460 nm, slits: 2 nm/2 nm. (b) Colour changes after the detection under visible-light. (c) Pictures of TLC plates under 365 nm light. Spots (a~d) on the TLC plates were probe **QX9A-Pd**, fluorophore **QX9A**, reaction mixture of probe with $Pd(PPh_3)_2Cl_2$ in the absence and in the presence of $NaBH_4$, respectively.

9.3 Detection of $Pd(dppf)Cl_2$

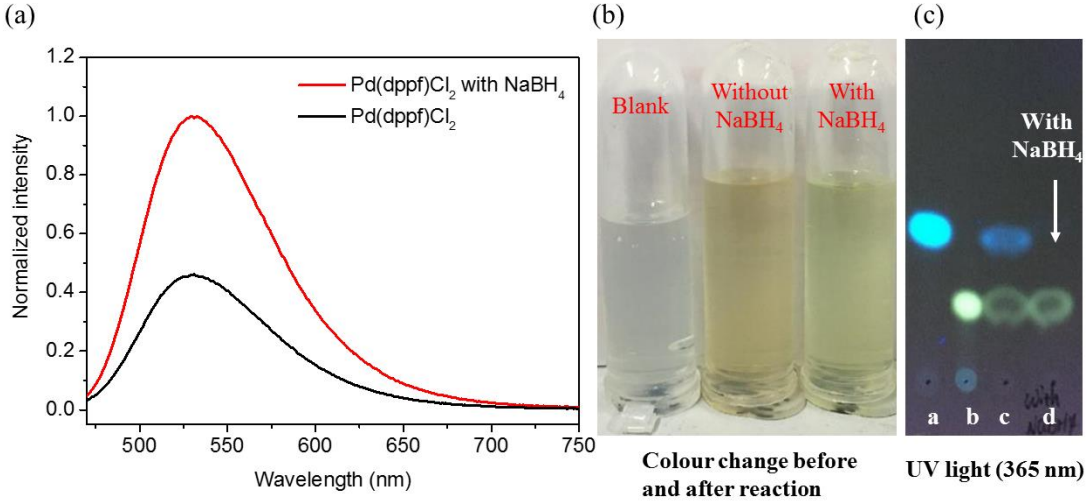

Fig. S10 (a) Fluorescence spectra changes of probe **QX9A-Pd** in the presence or absence of $NaBH_4$ when detecting $Pd(dppf)Cl_2$. Each spectrum was obtained in pH= 7.4 PBS buffer and PEG400 solutions (PBS: PEG400 = 40: 60, v/v) at 37 ºC for 1 h. λ_{ex}= 460 nm, slits: 2 nm/2 nm. (b) Colour changes after the detection under visible-light. (c) Pictures of TLC plates under 365 nm light. Spots (a~d) on the TLC plates were probe **QX9A-Pd**, fluorophore **QX9A**, reaction mixture of probe with $Pd(dppf)Cl_2$ in the absence and in the presence of $NaBH_4$, respectively.

9.4 Detection of $PdCl_2$

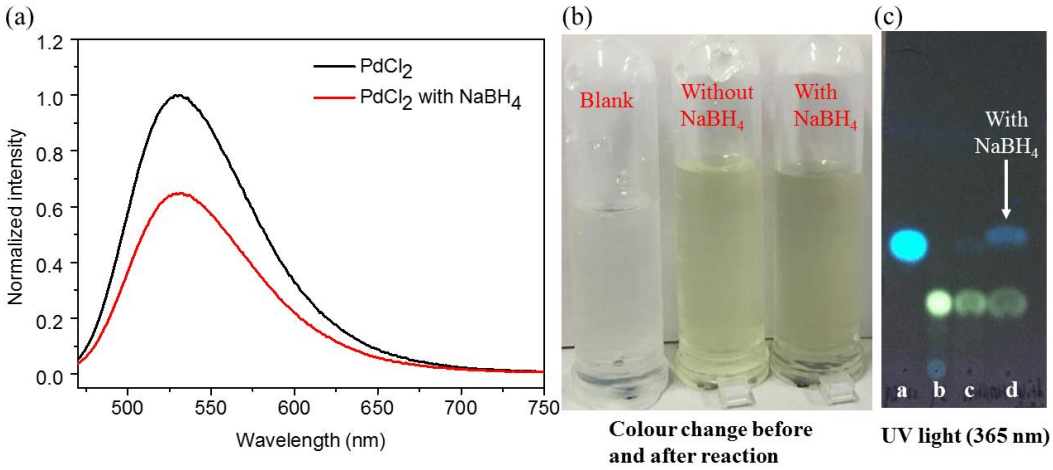

Fig. S11 (a) Fluorescence spectra changes of probe **QX9A-Pd** in the presence or absence of $NaBH_4$ when detecting $PdCl_2$. Each spectrum was obtained in pH= 7.4 PBS buffer and PEG400 solutions (PBS: PEG400 = 40:60, v/v) at 37 ºC for 1 h. λ_{ex}= 460 nm, slits: 2 nm/2 nm. (b) Colour changes after the detection under visible-light. (c) Pictures of TLC plates under 365 nm light. Spots (a~d) on the TLC plates were probe **QX9A-Pd**, fluorophore **QX9A**, reaction mixture of probe with $PdCl_2$ in the absence and in the presence of $NaBH_4$, respectively.

9.5 Detection of K_2PdCl_6

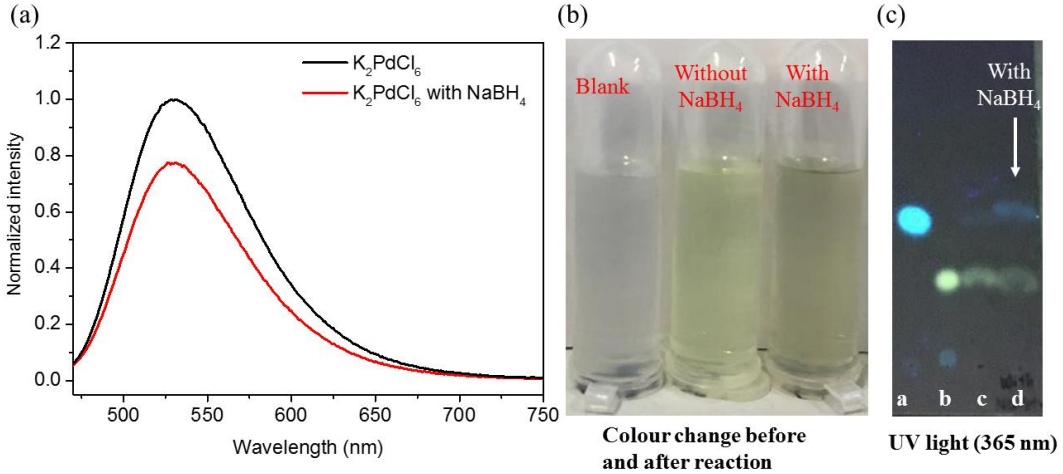

Fig. S12 (a) Fluorescence spectra changes of probe **QX9A-Pd** in the presence or absence of $NaBH_4$ when detecting K_2PdCl_6. Each spectrum was obtained in pH= 7.4 PBS buffer and PEG400 solutions (PBS: PEG400 = 40:60, v/v) at 37 °C for 1 h. λ_{ex}= 460 nm, slits: 2 nm/2 nm. (b) Colour changes after the detection under visible-light. (c) Pictures of TLC plates under 365 nm light. Spots (a~d) on the TLC plates were probe **QX9A-Pd**, fluorophore **QX9A**, reaction mixture of probe with K_2PdCl_6 in the absence and in the presence of $NaBH_4$, respectively.

10. Real sample analysis

The Pd^{2+} content in actual water samples included the Xuanwu Lake and tap water from Nanjing City, Jiangsu Province. All water samples were filtered through a 0.22 μm filter membrane to remove some impurities of large particles. According to the previous reported method[6-10], different amounts of $PdCl_2$ were spiked into the tap water and lake water, respectively. The intensity for each of the four solutions was determined at 532 nm for the fluorescence spectrum. The results were obtained and the working curve was prepared. The intensity of the sample solutions was determined to find out the concentration of Pd^{2+} by the working curve method.

Table S2 Application in practical samples detection for Pd^{2+}.

Sample	Pd^{2+} added (μM)	Pd^{2+} determined (μM)	Recovery (%)
Tap water	1.00	1.09	109.0
	2.00	2.06	103.2
	5.00	4.92	98.3
	10.00	9.66	96.6
Xuanwu Lake	1.00	1.08	107.9
	2.00	2.10	105.0
	5.00	5.15	102.9
	10.00	10.22	102.2

11. Stability test

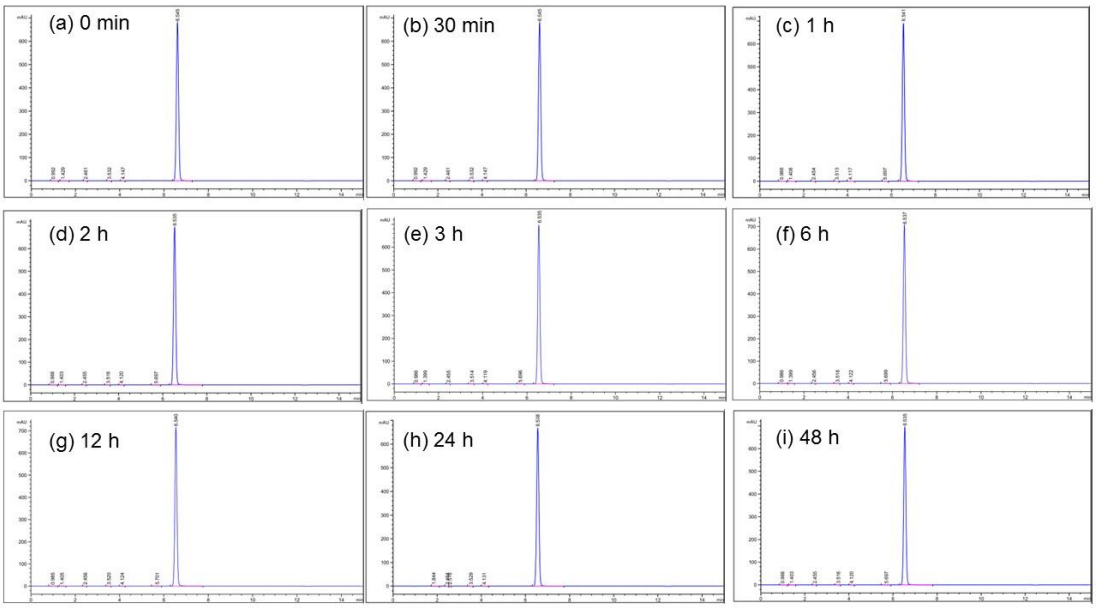

Fig. S13 Stability examination of probe **QX9A-Pd** (1 mg/mL) in pH= 7.4 PBS buffer and PEG400 solutions (PBS: PEG400 = 40: 60, v/v).

Before the intracellular application, a short investigation on the stability of probe **QX9A-Pd** was performed under both extended photochemical conditions and the testing conditions. The stability test was carried out in pH= 7.4 PBS buffer and PEG400 solutions (PBS: PEG400 = 40: 60, v/v) and the solutions were exposed to the light (λ= 365 nm). The stability of the probe was investigated by HPLC in each interval individually (Fig. S13). Indeed, probe **QX9A-Pd** remain same from 0 to 48 h in the solution and no new peaks were detected by HPLC. Hence, the probe was stable under both extended photochemical conditions and the testing conditions.

12. Cytotoxicity assays of probe QX9A-Pd at different concentrations

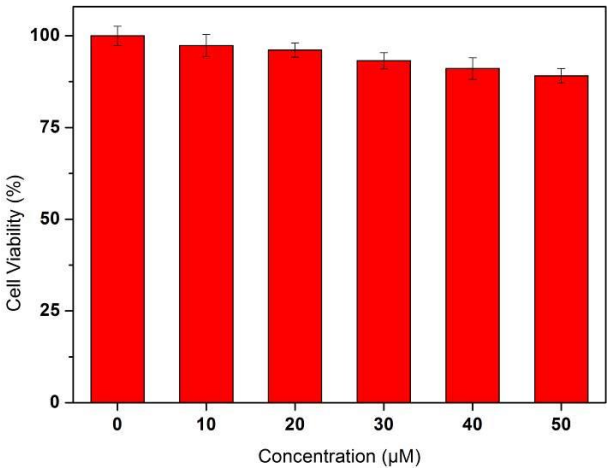

Fig. S14 MTT assay for the survival rate of HeLa cells treated with various concentrations of probe **QX9A-Pd** for 24 h. MTT: 3-(4,5-dimethylthiazol-2-yl)-2,5-diphenyltetrazolium bromide, thiazolyl blue.

13. Palladium detection with QX9A-Pd in living cells

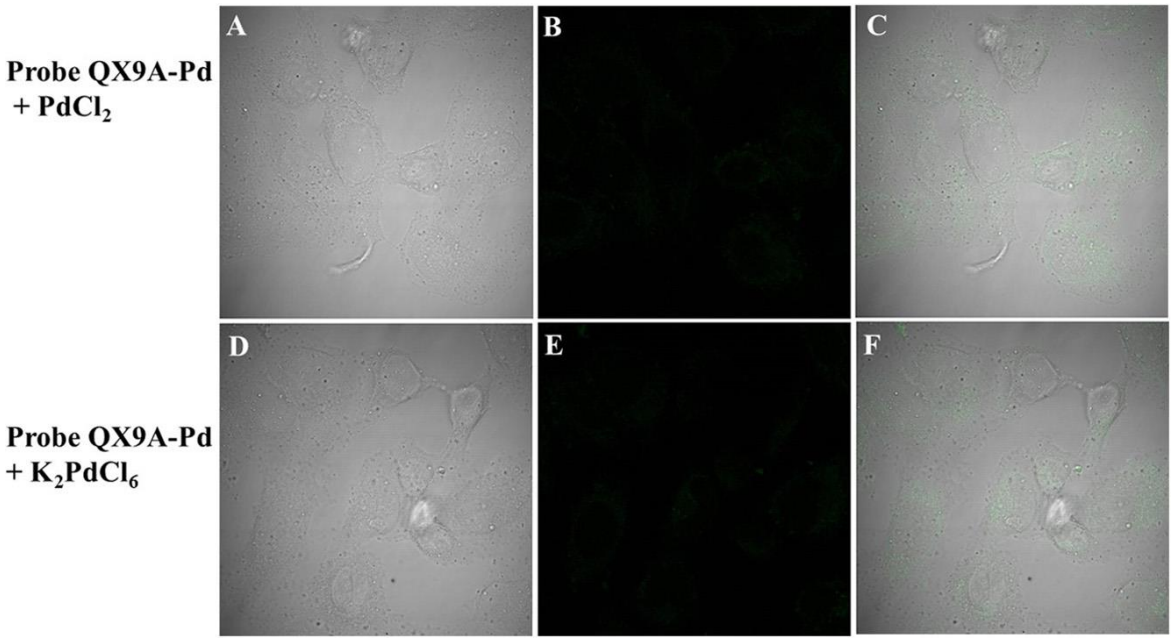

Fig. S15 (A-C) Imaging of HeLa cells treated with **QX9A-Pd** for 30 min followed by 50 μM $PdCl_2$ for another 30 min; (D-F) imaging of HeLa cells treated with QX9A-Pd for 30 min followed by 50 μM K_2PdCl_6 for another 30 min. (Left) Bright-field image; (middle) fluorescence image; (right) merged image.

14. Reported fluorescent probes

Table S3 Comparison of fluorescent probes for palladium detection

Probe	$\lambda_{ex}/\lambda_{em}$ (nm)	Detection limit	Detection medium	Target	Notes	Reference
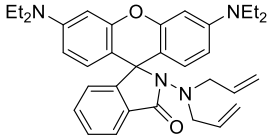	530/580	185 nM	EtOH:H_2O (1: 1, v/v)	Pd(0) and Pd(II)	Coordination mechanism	Chem. Commun., 2010, 46: 1079-1081
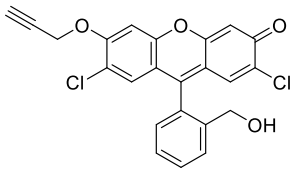	480/520	30 nM	CH_3CN:H_2O (1:9, v/v)	Pd(0), Pd(II) and Pd(IV)	No additional reagents	Chem. Commun., 2010,46: 3964-3966
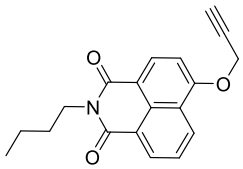	410/480 410/553	70 nM	PBS (20 mM, pH 7.4)	Pd(0), Pd(II) and Pd(IV)	No additional reagents	Chem. Commun. 2011, 47: 8656-8658

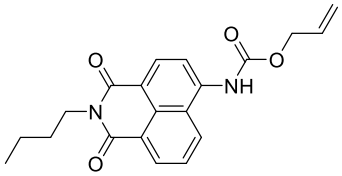	403/498 403/524	6.1 nM	$CH_3CN:H_2O$ (4:1, v/v)	Pd(0) and Pd(II)	Need $NaBH_4$-PPh_3, morpholine	Org. Lett. 2011, 13: 4922-4925
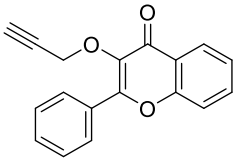	403/412 403/517	87 nM	CH_3CN: HEPES (1: 4, v/v, 10 mM)	Pd(0), Pd(II) and Pd(IV)	——	Chem. Commun., 2012,48: 2867-2869
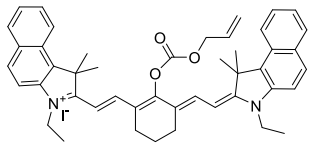	545/810 545/655	2.7 nM	CH_3CN:PBS (1:3, v/v, pH = 7.4, 10 mM)	Pd(0)	——	Chem. Commun., 2014,50: 13525-13528
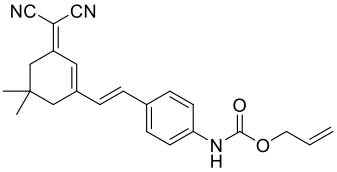	472/570 472/643	24.2 nM	DMSO:PBS (1:1, v/v, pH = 7.4, 20 mM)	Pd(0)	——	RSC Adv., 2015,5: 52516-52521
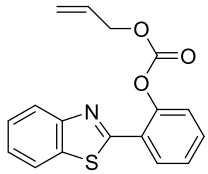	325/420 325/476	15.6 nM	CH_3CN:PBS (1:9, v/v, pH = 7.4, 10 mM)	Pd(0), Pd(II) and Pd(IV)	$NaBH_4$ was needed for detecting Pd(II) and Pd(IV)	J. Mater. Chem. B, 2016, 4: 3911-3915
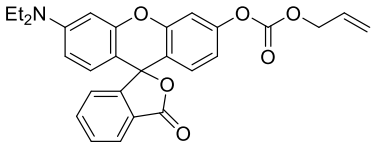	500/547	1.14 nM	THF:PBS (1:1, v/v, pH = 7.4, 20 mM)	Pd(0)	——	J. Photochem. Photobiol. A Chem. 2017, 337: 25-32
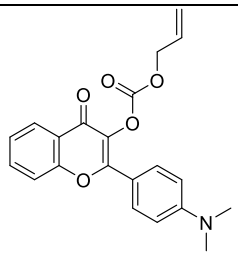	380/470 380/552	90 nM	THF:PBS (1:9, v/v, pH = 7.4, 20 mM)	Pd(0), Pd(II) and Pd(IV)	$NaBH_4$ was needed for detection	Org. Biomol. Chem., 2017,15: 5846-5850
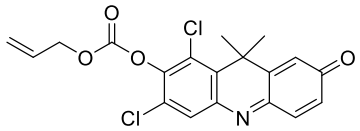	602/665	2.2 nM	DMSO:PBS (1:4, v/v, pH 7.4) or PBS	Pd(0), Pd(II) and Pd(IV)	PPh_3 was needed for detecting Pd(II) and Pd(IV)	Sensors and Actuators B, 2018, 258: 98-104
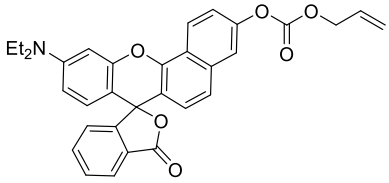	564/636	1.6 nM	PBS buffer (10 mM, pH 7.4)	Pd(0), Pd(II) and Pd(IV)	PPh_3 was needed for detecting Pd(II) and Pd(IV)	Dyes Pigm. 2018, 152:112-117

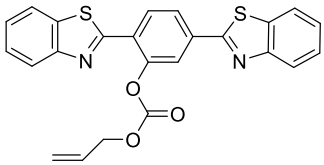	350/411 350/523	44 nM	HEPES: EtOH (3:2, v/v, 10 mM, pH = 7.4)	Pd(0) and Pd(II)	$NaBH_4$ was needed for detecting Pd(II)	Inorg. Chim. Acta, 2019, 495: 119000.
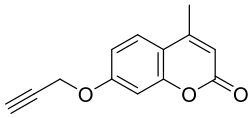	322/380 322/450	1.1 nM	CH_3CN:PBS (1:9, v/v, pH = 7.4, 10 mM)	Pd(II)	Selective detection of Pd(II) from Pd(0)	Spectrochim. Acta A: 2019, 220, 117134.
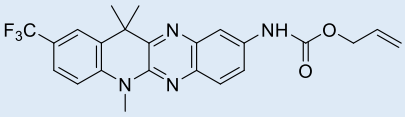	460/532	29.0 nM for $Pd(PPh_3)_4$, 29.4 nM for $PdCl_2$ and 34.0 nM for K_2PdCl_6	PEG400:PBS (3:2, v/v, pH = 7.4, 10 mM), no $NaBH_4$	Pd(0), Pd(II) and Pd(IV)	1. With PEG400: detect Pd(0), Pd(II) and Pd(IV); 2. Without PEG400: selectivity towards Pd(0).	This work

15. NMR and Mass spectra of compounds

15.1 The characterization of intermediate **QX8N**

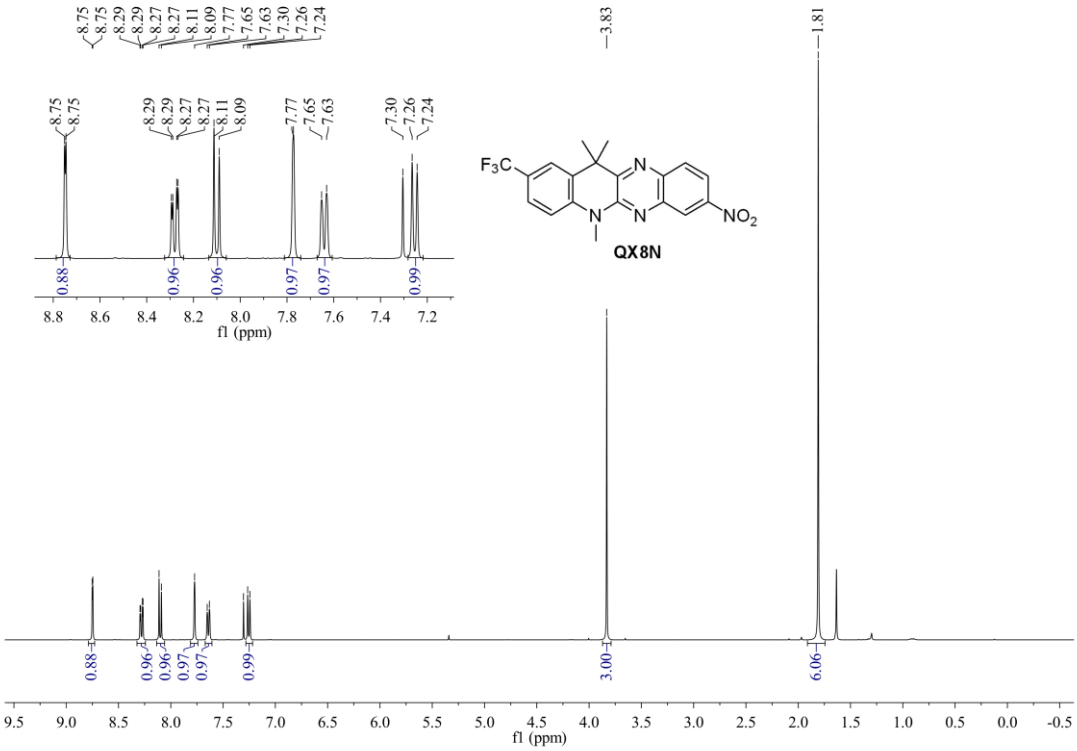

^{1}H NMR spectrum of intermediate **QX8N** in $CDCl_3$.

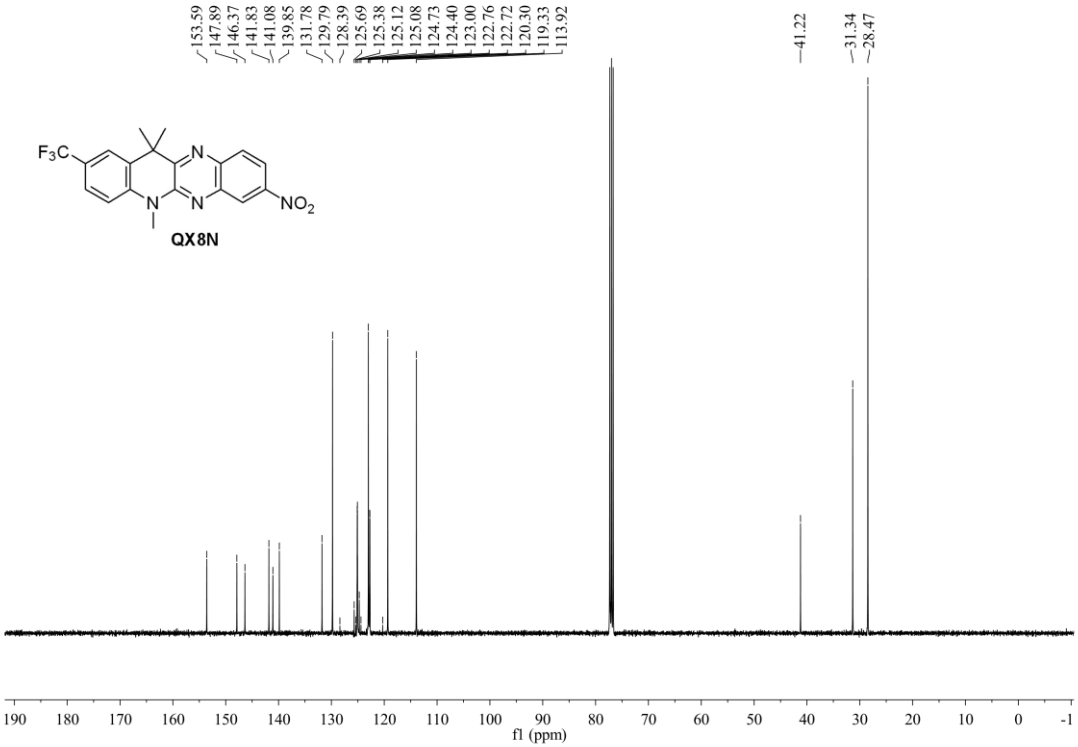

^{13}C NMR spectrum of intermediate **QX8N** in $CDCl_3$.

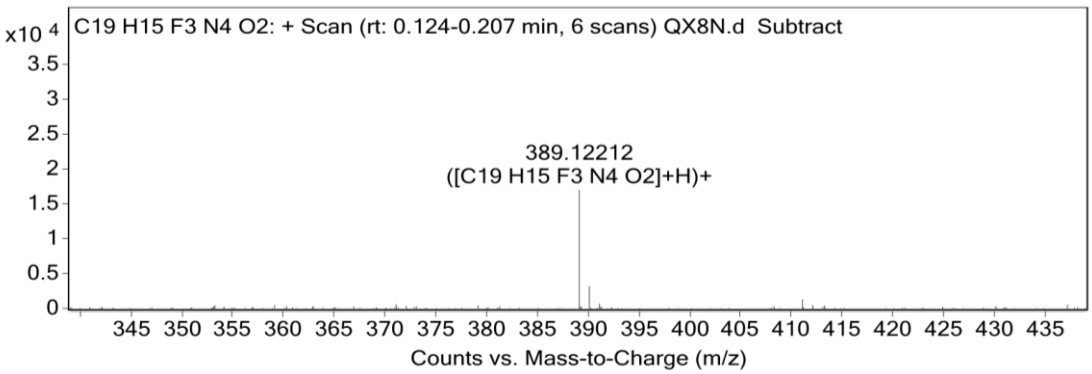

HR-MS spectrum of intermediate **QX8N**

15.2 The characterization of intermediate **QX9N**

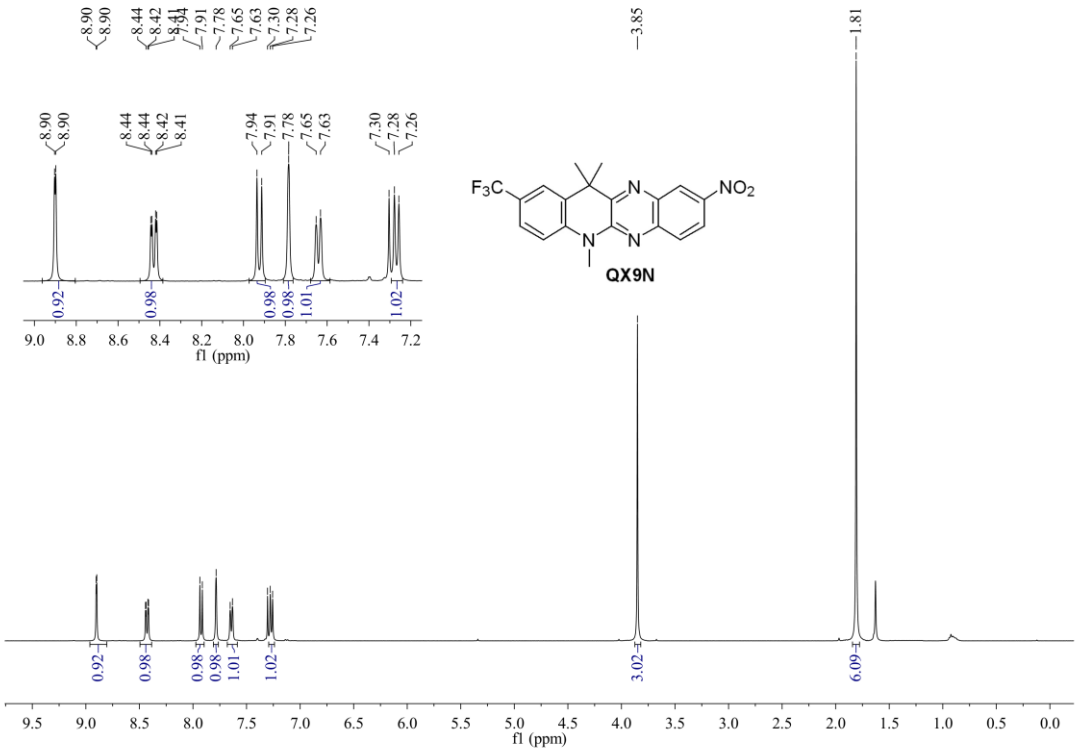

^{1}H NMR spectrum of intermediate **QX9N** in $CDCl_3$.

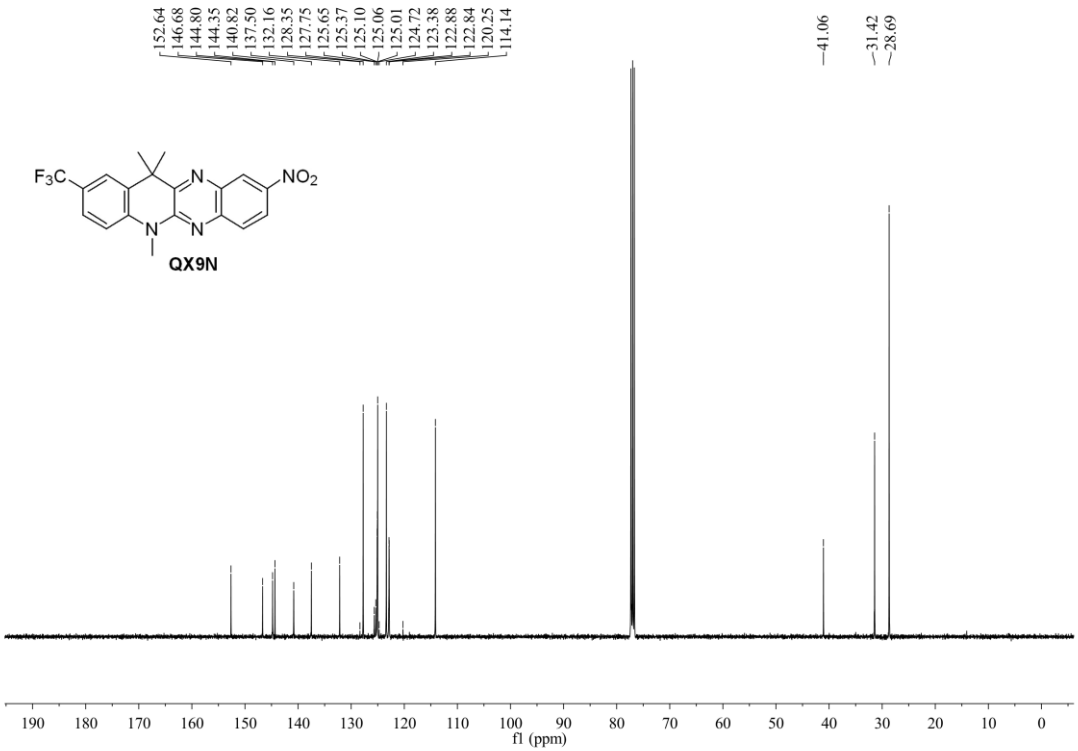

^{13}C NMR spectrum of intermediate **QX9N** in $CDCl_3$.

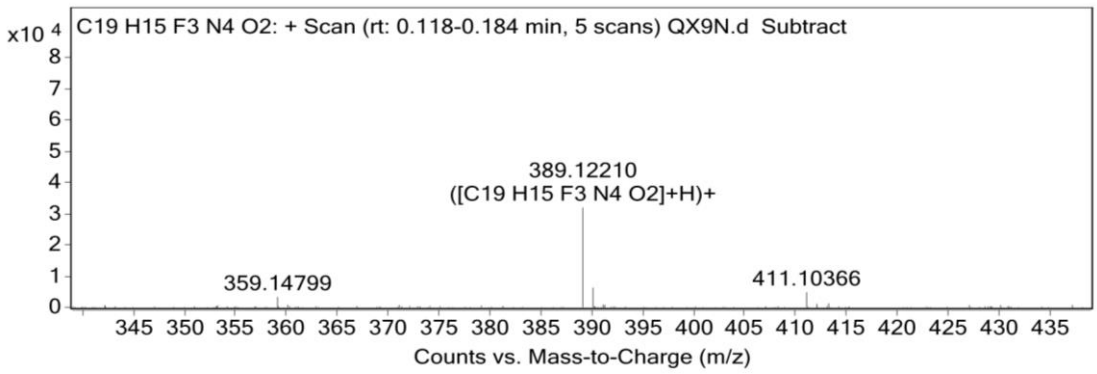

HR-MS spectrum of intermediate **QX9N**

15.3 The characterization of fluorophore **QX8A**

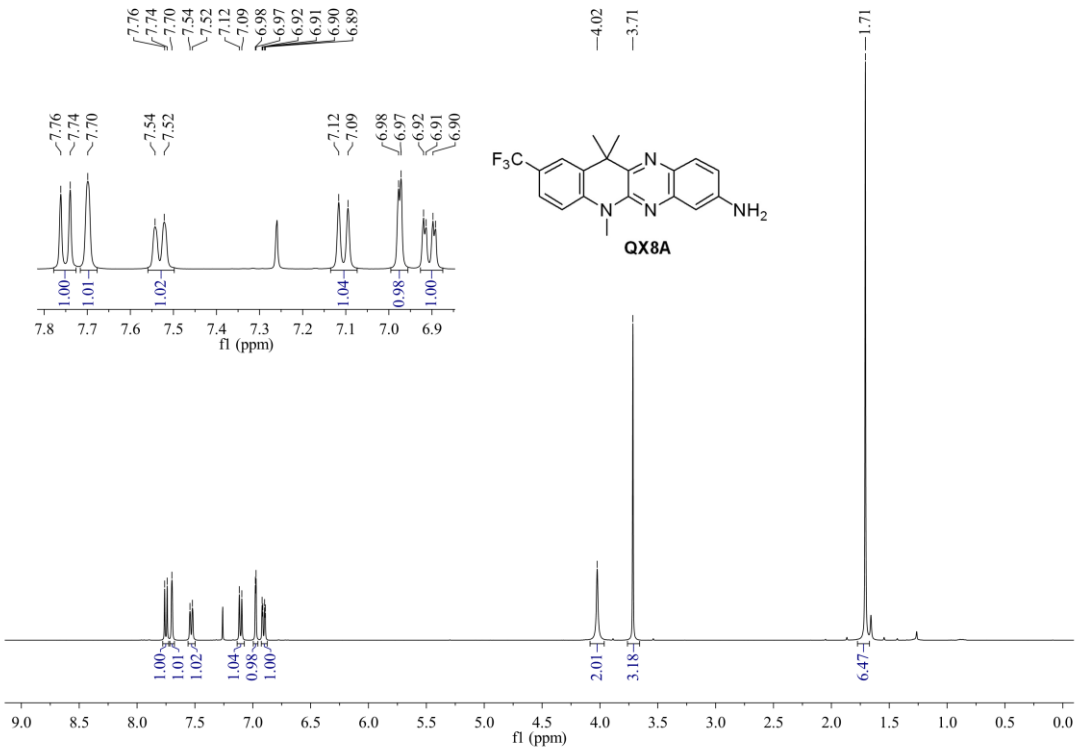

^{1}H NMR spectrum of fluorophore **QX8A** in $CDCl_3$.

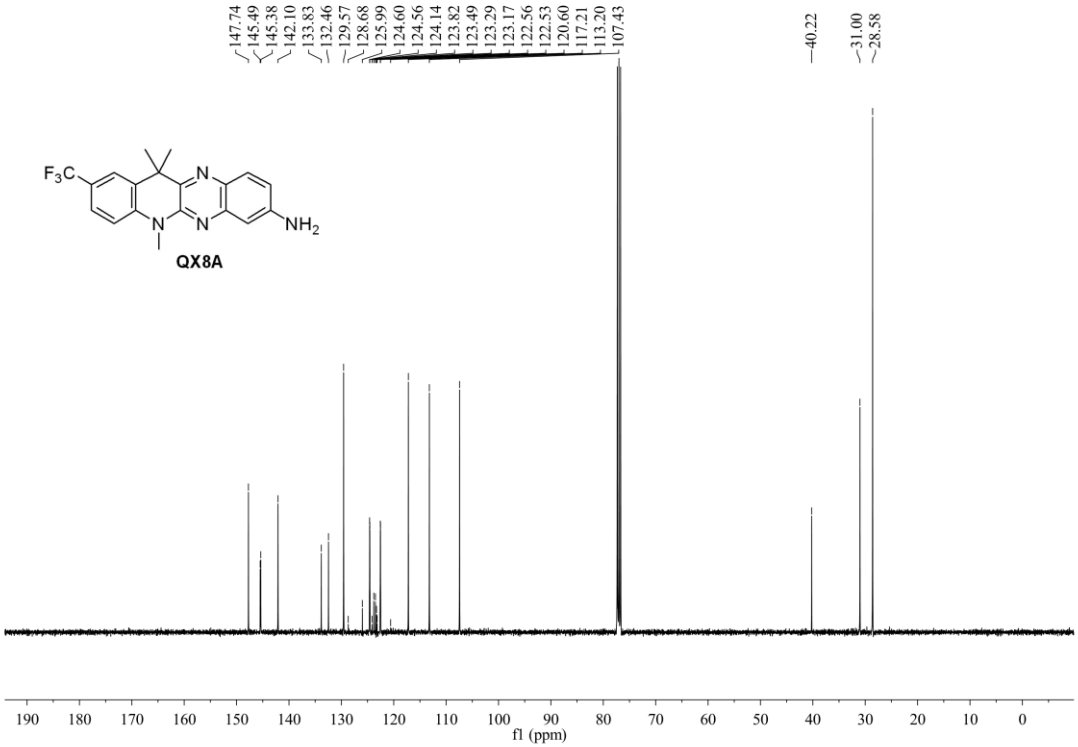

^{13}C NMR spectrum of fluorophore **QX8A** in $CDCl_3$.

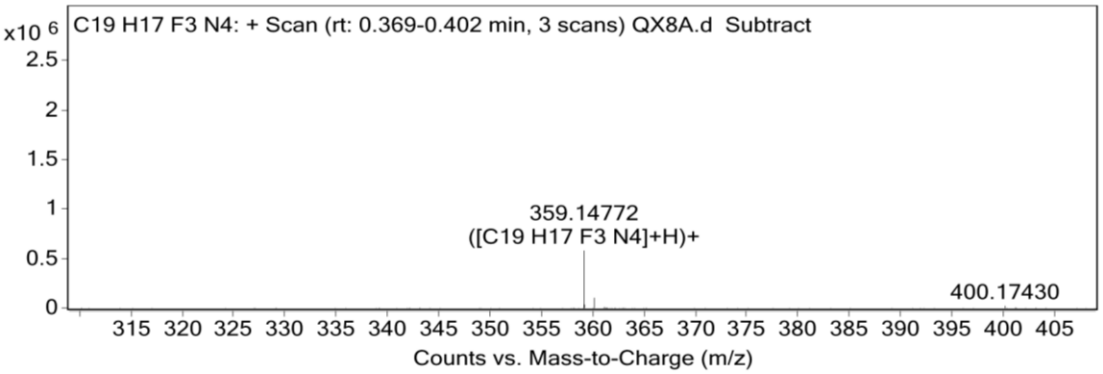

HR-MS spectrum of fluorophore **QX8A**

15.4 The characterization of fluorophore **QX9A**

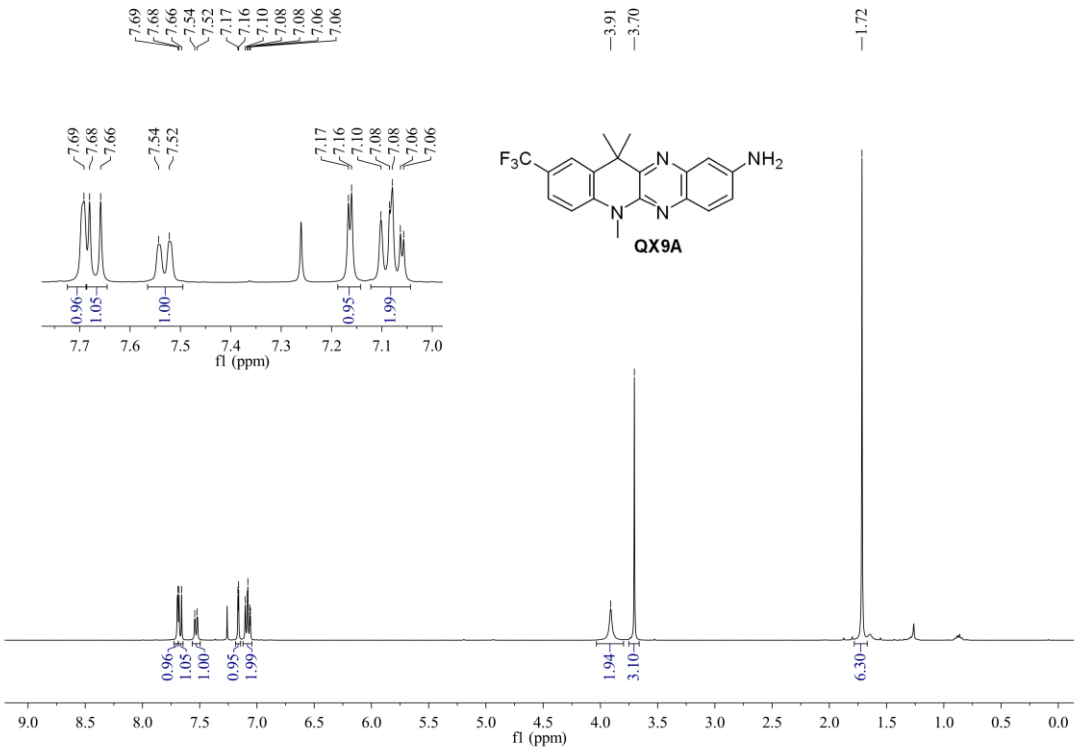

^{1}H NMR spectrum of fluorophore **QX9A** in $CDCl_3$.

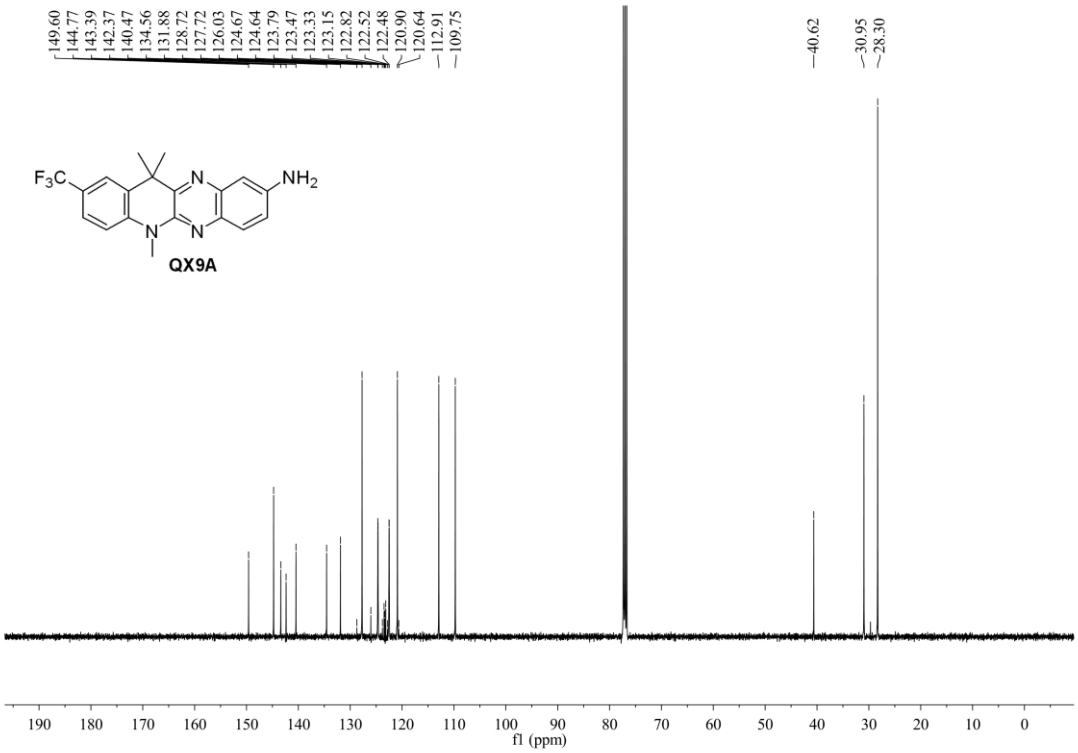

^{13}C NMR spectrum of fluorophore **QX9A** in $CDCl_3$.

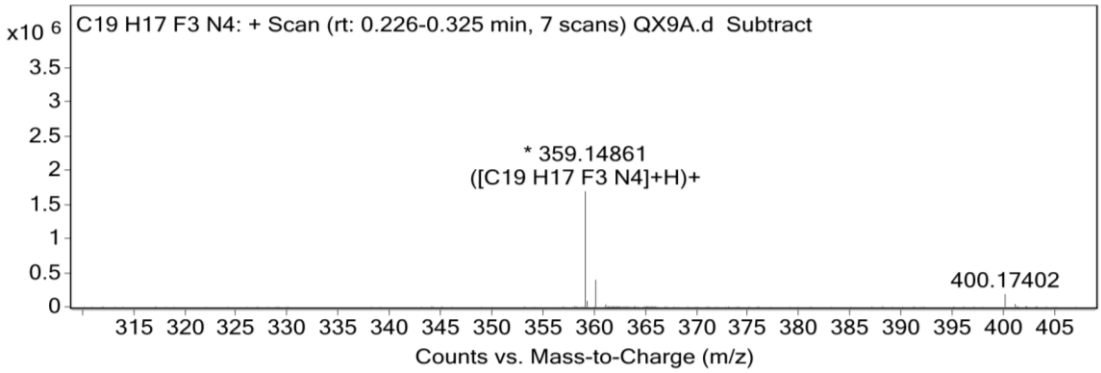

HR-MS spectrum of fluorophore **QX9A**

15.5 The characterization of probe **QX8A-Pd**

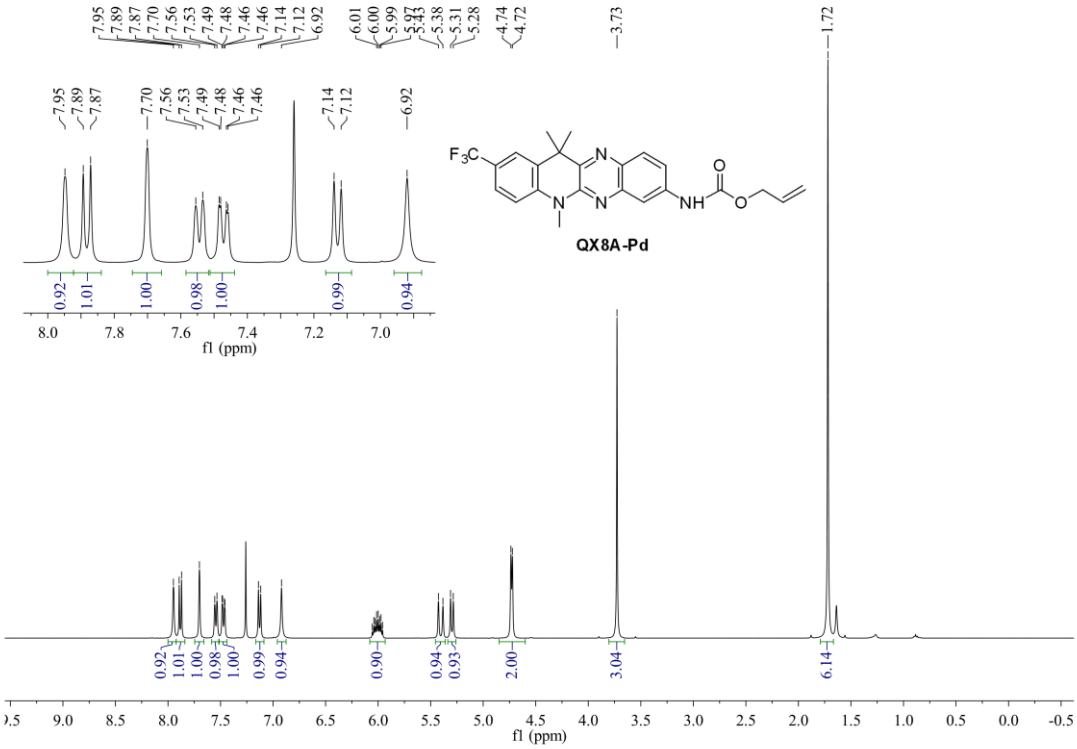

^{1}H NMR spectrum of probe **QX8A-Pd** in $CDCl_3$.

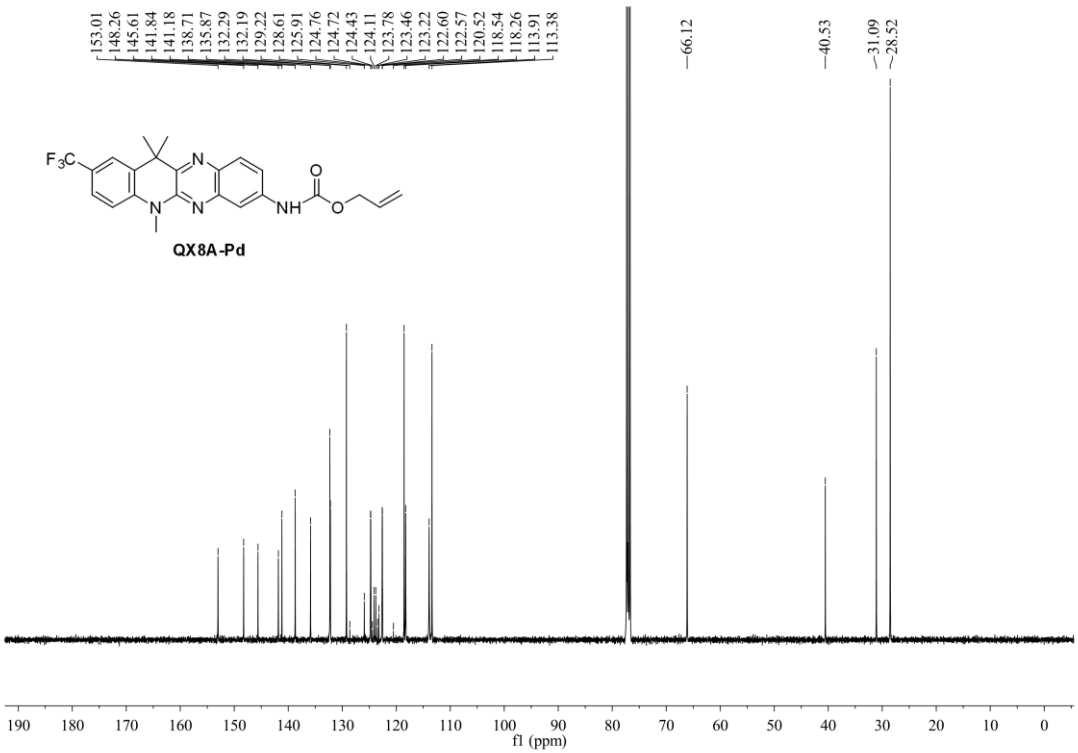

^{13}C NMR spectrum of probe **QX8A-Pd** in $CDCl_3$.

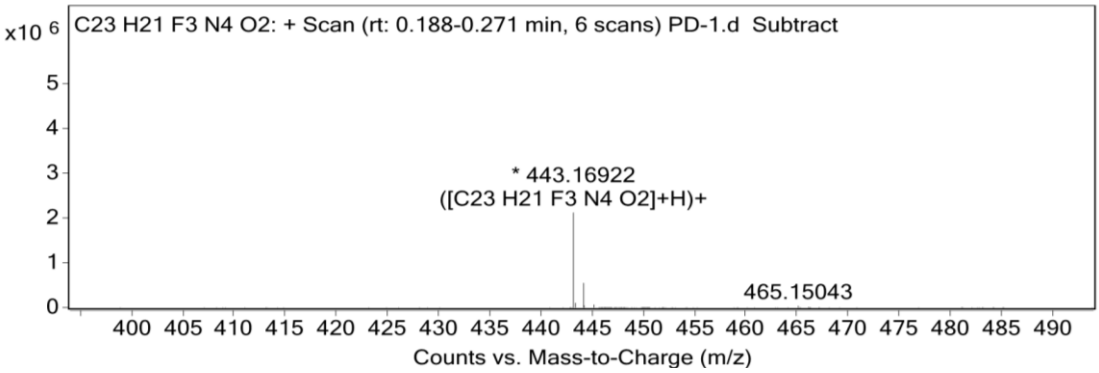

HR-MS spectrum of probe **QX8A-Pd**

15.6 The characterization of probe **QX9A-Pd**

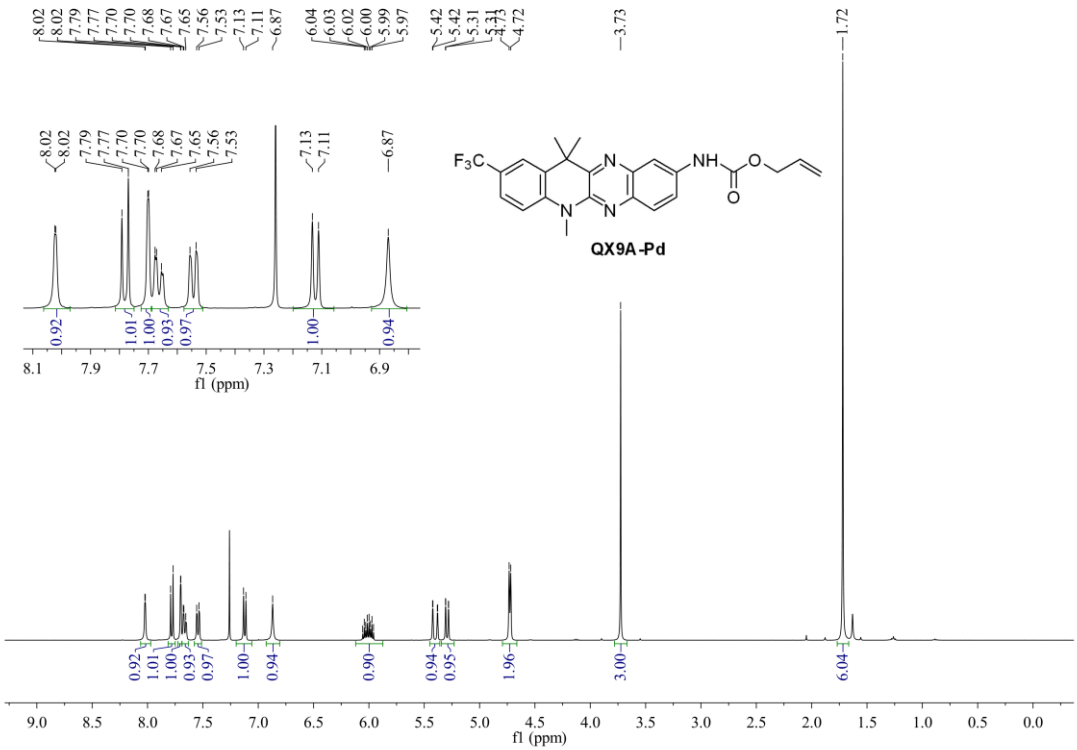

^{1}H NMR spectrum of probe **QX9A-Pd** in $CDCl_3$.

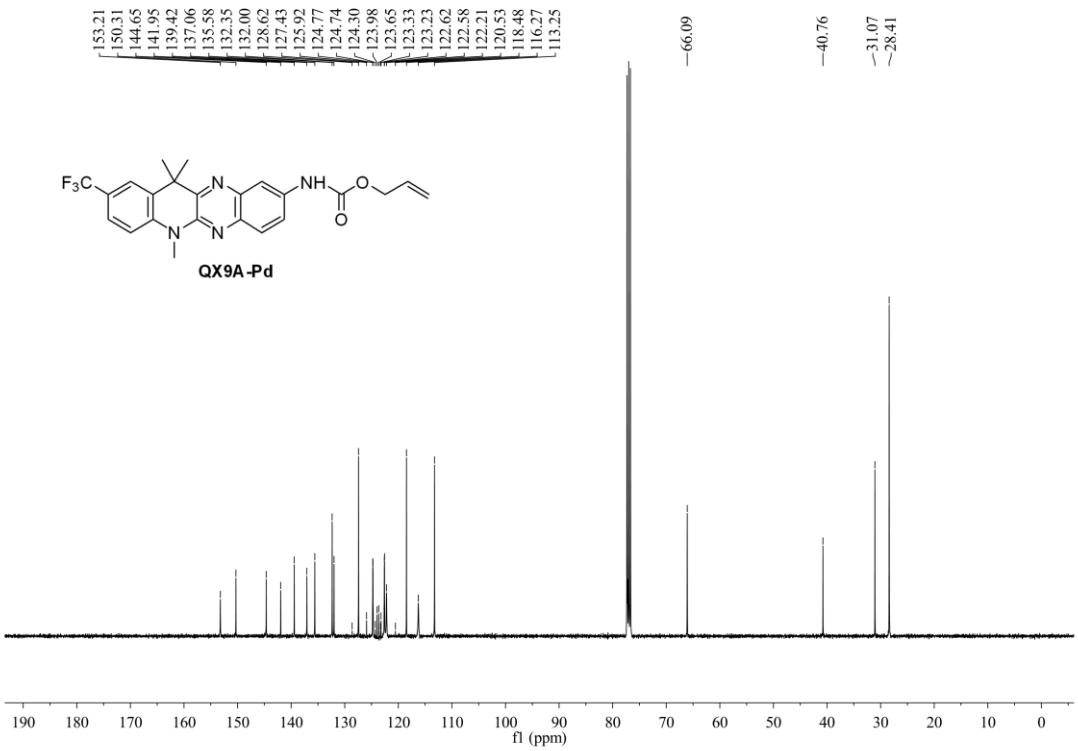

^{13}C NMR spectrum of probe **QX9A-Pd** in $CDCl_3$.

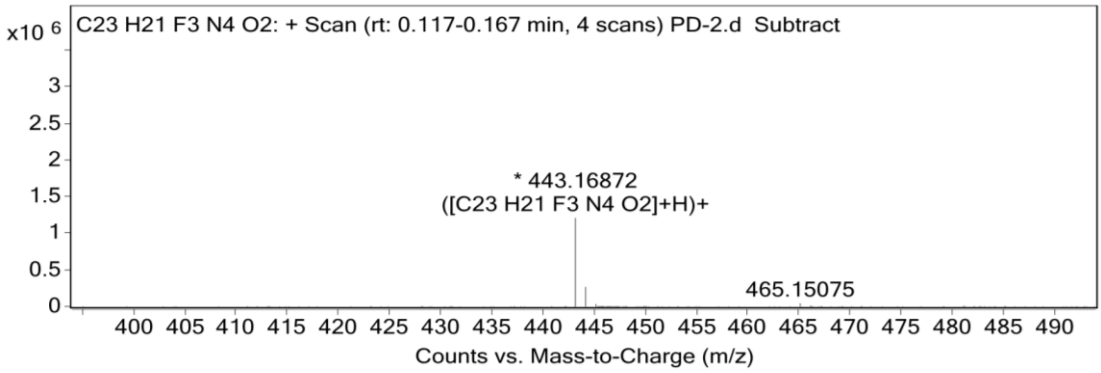

HR-MS spectrum of probe **QX9A-Pd**

16. References

[1] Hopkins P A, Sinkeldam R W, Tor Y. Visibly emissive and responsive extended 6-aza-uridines[J]. Org Lett, 2014, 16(20): 5290-5293.

[2] Li H, Luan Z, Zheng G, et al. Efficient synthesis of chiral indolines using an imine reductase from *Paenibacillus lactis*[J]. Adv Synth Catal, 2015, 357(8): 1692-1696.

[3] Liu H, Chen H, Li Y, et al. A novel and one-pot method for synthesis of unprecedented 3,3-dimethyl-2-amide indoles under metal-free conditions[J]. Tetrahedron Lett, 2015, 56(18): 2332-2335.

[4] Owens E A, Hyun H, Dost T L, et al. Near-infrared illumination of native tissues for image-guided surgery[J]. J Med Chem, 2016, 59(11): 5311-5323.

[5] Zhang Y, Yang M, Jia C, et al. Iodine-promoted domino oxidative cyclization for the one-pot synthesis of novel fused four-ring quinoxaline fluorophores by sp^3 C−H functionalization[J]. Chem Eur J, 2019, 25(60): 13709-13713.

[6] Wu X, Chen J, Zhao J X. A reversible fluorescent logic gate for sensing mercury and iodide ions based on a molecular beacon[J]. Analyst, 2013, 138(18): 5281-5287.

[7] Qu S, Zheng C, Liao G, et al. A fluorescent chemosensor for Sn^{2+} and Cu^{2+} based on a carbazole-containing diarylethene[J]. RSC Adv, 2017, 7(16): 9833-9839.

[8] Wang Z, Cui S, Qiu S, et al. A dual-functional fluorescent sensor based on diarylethene for Zn^{2+} and Al^{3+} in different solvents[J]. J Photochem Photobiol A: Chem, 2019, 376: 185-195.

[9] Wang Z, Cui S, Qiu S, et al. A novel diarylethene-based fluorescent “turn-on” sensor for the selective detection of Mg^{2+}[J]. RSC Adv, 2019, 9(11): 6021-6026.

[10] Wang Z, Cui S, Qiu S, et al. A highly selective fluorescence “turn-on” sensor for Ca^{2+} based on diarylethene with a triazozoyl hydrazine unit[J]. RSC Adv, 2018, 8(51): 29295-29300.